VIP Iron Biomineralization

DOI: 10.1002/ange.200705723

Periodic Iron Nanomineralization in Human Serum Transferrin Fibrils**

Surajit Ghosh, Arindam Mukherjee, Peter J. Sadler, and Sandeep Verma**

Life exists now in an oxidizing environment, and extracellular iron is largely present as Fe^{III} rather than Fe^{II}. Aqua Fe^{III} ions are acidic and readily form hydroxo and oxo species in aqueous solution. Hydroxide and oxide are good bridging ligands, and so hydrolysis can give rise to relatively insoluble polymeric hydroxo/oxo Fe^{III} precipitates. Iron biomineralization occurs in natural biological processes.[1,2] For example, iron is stored in ferritin as a form of ferrihydrite, and magnetotactic bacteria use magnetite particles as navigational aids. On the other hand, controlled mineralization in biological systems can be deleterious and is thought to be involved in the pathogenesis of various neurodegenerative diseases.[3] Hence, the transport and deposition of iron in biological systems is carefully controlled, mainly by specialized proteins.

Iron is transported in human blood as Fe^{III} tightly bound to the 80-kDa bilobal glycoprotein transferrin, present at a concentration of about 35 μM.[4–6] Human serum transferrin (hTf) contains two Fe^{III} sites, one in each lobe. In contrast, Fe^{II} binds very weakly. Octahedral high-spin Fe^{III} is bound to four amino acid side chains (two tyrosinates, one aspartate, and one histidine) and to a bidentate carbonate ion, the so-called synergistic anion. Bound Fe^{III} is situated in a closed cleft, hinged at the back by antiparallel β strands.[7] Hydrogen-bonding interactions between the protein and bound carbonate play important roles in stabilizing the closed cleft. Hinging allows the cleft to open so that iron can be released after Fe_2-hTf is taken up by cells. The bacterial analogue of hTf is the single-lobe protein ferric-ion-binding protein (Fbp). This protein has been shown to bind not only Fe^{III} in a closed-cleft mononuclear site, but also clusters of three to five metal ions (Fe^{III}, Hf^{IV}, Zr^{IV}) in an open cleft.[8–10] Cluster binding has yet to be demonstrated for hTf, although work on Hf^{IV} has suggested that this might be possible.[11] Herein we present the remarkable finding that human transferrin readily forms protein fibrils and in doing so gives rise to periodic iron nanomineralization along the length of the fibrils.

First, we investigated the ultrastructure of holo-Fe_2-hTf deposited on surfaces using various types of microscopy. Optical images of freshly prepared solutions of holo-hTf (1 μM in water) deposited on a glass surface indicated the propensity of holo-hTf to aggregate, leading to fiber formation (see Figure S1 in the Supporting Information). Aging of the transferrin solutions (for 0–7 days at 37 °C) and the concentration of holo-hTf (1–20 μM) had little influence on the images observed. Morphological studies of holo-hTf on copper stubs by scanning electron microscopy (SEM) revealed fibrillar growth with a tubular organization (Figure 1 A,B). The twisting of the sheets of fibers observed in Figure 1 D suggests the presence of helical chirality in the assembly.[12] Such twisting of strands is a feature of sickle hemoglobin fibers. Typically these consist of 20 to 200 double strands of hemoglobin molecules which can grow to indefinite lengths and are stabilized by intermolecular interactions around the single amino acid mutation at position β6 (glutamic acid to valine). Twisting produces axial strains that determine the pitch of the helix, which is also related to the diameter of the fibers.

Atomic force microscopy (AFM) further confirmed extensive fiber formation and revealed finer structural details of the fibers formed on mica surfaces from 1 μM holo-hTf solutions in 25 mM bicarbonate buffer (pH 8.21). At this high salt concentration, the formation of fibrous network was considerably masked with salt clusters (see Figure S2 in the Supporting Information). Typically, from solutions of holo-hTf in water, protein fibers with a width of approximately 24 Å were observed fused together to form thick fibrous bundles (Figure 1 C,D and Figure S3 in the Supporting Information). AFM images of holo-hTf (1 μM) in bicarbonate buffer (1–5 mM $NaHCO_3$, pH 7.22–7.44) also displayed similar fibrous morphology with a fiber cross section of approximately 80 Å (Figure 1 E,F).

Further insight into fiber morphology was achieved with transmission electron microscopy (TEM). Fresh aqueous holo-hTf solutions deposited on formvar-coated copper grids afforded fibrous structures in TEM micrographs, but

[*] Dr. A. Mukherjee, Prof. Dr. P. J. Sadler
Department of Chemistry
University of Warwick
Coventry (UK)
Fax: (+44) 247-652-3819
E-mail: p.j.sadler@warwick.ac.uk
Homepage: http://go.warwick.ac.uk/sadlergroup/
S. Ghosh, Prof. Dr. S. Verma
Department of Chemistry
Indian Institute of Technology
Kanpur, UP (India)
Fax: (+91) 512-259-7436
E-mail: sverma@iitk.ac.in
Homepage: http://home.iitk.ac.in/~sverma

[**] We thank the European Commission (Marie Curie Fellowship for A.M.) RCUK (Rasor, University of Edinburgh), IIT Kanpur (pre-doctoral fellowship for S.G.), and DST India (Swarnajayanti Fellowship for S.V.) for support; Dr. Dominic Campopiano, Dr. Paul Bilton, Dr. Ana Pizarro, and Dr. C. Logan Mackay for their kind assistance with instrumentation; and Prof. A. Sharma and ACMS IIT Kanpur for access to AFM and TEM and SEM-EDX analysis, respectively. We also thank Allen Hill (Oxford), Tiffany Walsh, Vilmos Fulop, Matthew Turner and Julie Macpherson (Warwick) for their comments on the script.

Supporting information for this article is available on the WWW under http://www.angewandte.org or from the author.

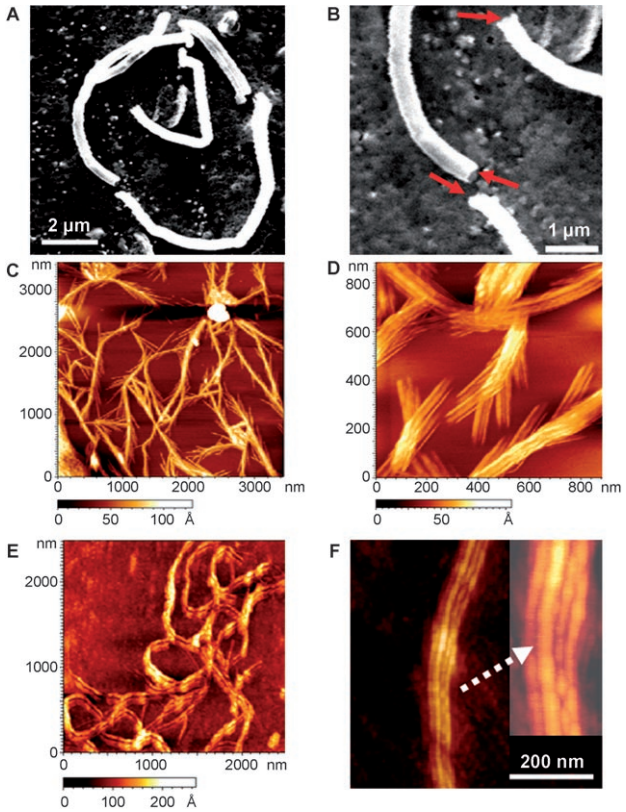

Figure 1. A, B) SEM images of aqueous holo-hTf. A) SEM image showing tubular structures. B) Magnified view of the tubular structure; red arrows indicate tubular endings. The solution of holo-hTf had been left to age for two days, but in general aging had little effect on the observed morphologies. C, D) AFM images of 1 μM aqueous holo-hTf after drying on freshly cleaved mica surface. C) Extensive fibrous networks. D) Magnified view of thin fused fibers. E) Fibrillation in 1 μM holo-hTf solution in bicarbonate buffer (1 mM $NaHCO_3$, pH 7.22). F) Magnified views of a fused fiber in (E).

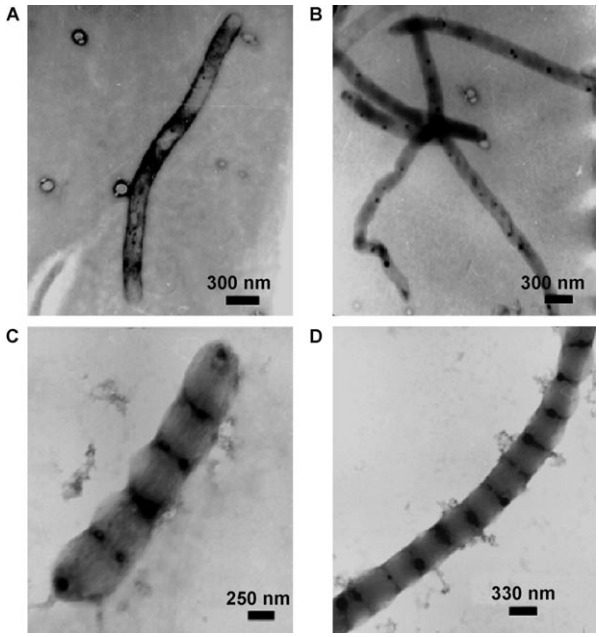

Figure 2. TEM images from 1 μM holo-hTf solutions after drying on formvar-coated Cu grids. A) A representative fiber formed in aqueous hTf solution showing dark spots periodically arranged within the fiber. B) Multiple fibers containing electron-dense dark spots. C, D) Fibers from fresh solution in the bicarbonate buffer (1 mM $NaHCO_3$, pH 7.22) showing slightly different arrangement of dark spots with nearly uniform spacing along fiber lengths. Although the average width of the fibers (ca. 500 nm) is similar in (C) and (D), the spacing between the dark bands is larger in (C) (ca. 375 nm) than in (D) (ca. 250 nm).

interestingly, we also observed periodically aligned electron-dense dark spots along the fiber length (Figure 2 A,B and Figure S4 in the Supporting Information). Such uniformly spaced dark spots were also observed in fibers (of ca. 500 nm in diameter) from holo-hTf (1 μM) incubated in 1 mM bicarbonate buffer (Figure 2 C,D and Figure S5 in the Supporting Information). The periodicity of the spots was variable, for example, approximately 250-nm spacing between bands in Figure 2 C and approximately 375 nm in Figure 2 D. When apo-hTf solution was deposited on a similar surface, fiber formation was also observed, but without the occurrence of dark spots (see Figure S6 in the Supporting Information). This finding clearly suggests that the dark spots detected in holo-hTf fibers can be attributed to the presence of iron.

We then investigated the nature of these electron-dense regions (dark spots) by SEM/EDX (energy dispersive X-ray) analysis. A section of an holo-hTf fiber was selected from the SEM micrograph and subjected to EDX analysis. Although weak, an iron peak was observed from the selected region along with copper, zinc, and gold peaks obtained from the copper stub used and its gold plating prior to the SEM analysis (Figure S7). However, a strong iron peak was observed from a 30-day-aged aqueous solution of holo-hTf that had undergone extensive fibrillation (Figure 3 A). We then recorded the selected area diffraction pattern (SADP) from the dark spots (Figure 3 B,C). The SADP of a dark spot resembled the pattern from an iron mineral. The observed *d* values of 6.17, 3.24, 2.51, 1.849, 1.525, and 1.239 Å are close to those documented for the common Fe^{III} oxide/hydroxide mineral lepidocrocite, γ-Fe(O)(OH) (rust; *d* spacings: 6.26, 3.29, 2.47, 1.94, 1.73, 1.52 Å).[13,14] Therefore, it can be concluded that the dark spots along the length of the fibers result from nanomineralization involving migration of iron from the binding cleft of holo-hTf under the influence of aggregation and fibril formation.

In another set of experiments, apo-hTf was artificially loaded with Fe, Mn, or Bi ions, and these samples were analyzed for fiber formation by TEM. Apo-hTf reloaded using iron(III) nitrilotriacetate (Fe^{III}-NTA) also gave rise to dark spots within the fibers, although now, intriguingly, as much more localized spots (Figure 4 A). X-ray crystallographic studies have shown that reloading of ovotransferrin with Fe^{III}-NTA can lead to binding of Fe^{III}-NTA in an open cleft.[15] Therefore it is likely that hTf reloaded with iron in this way contains some molecules with Fe^{III} capped by NTA bound in the clefts of the protein. Hence the nanomineralization process may depend on the exact form of the iron bound in the protein cleft, a feature which could be important in vivo if other anions replace carbonate.

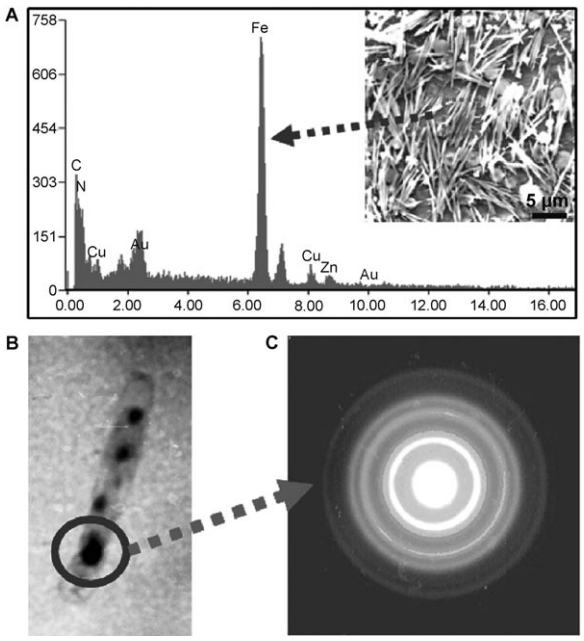

Figure 3. Detection of iron in transferrin fibers. A) EDX spectrum of 30-day-aged fibrous bundles from aqueous holo-hTf solution (1 μM); arrow indicates the iron peak and inset shows the area used to collect the EDX data. B) TEM image of a fiber. C) Selected area diffraction pattern of a dark spot in the fiber as indicated.

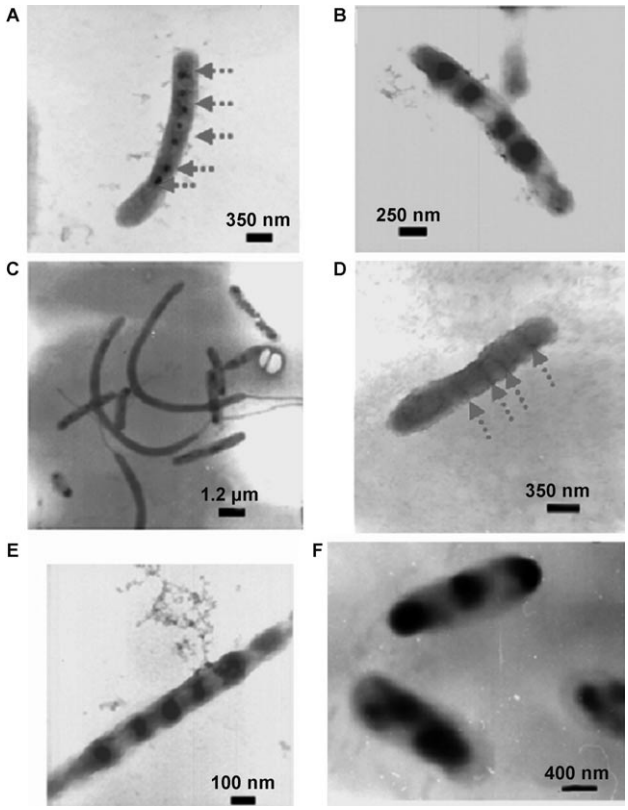

Figure 4. TEM images of iron, manganese, and bismuth hTf prepared by reloading apo-hTf, and of deglycosylated holo-hTf, in 5 mM NH_4HCO_3, pH 7.4. A) Artificially loaded Fe^{III}-hTf displaying prominent dark spots within a fiber. B) Mn-hTf showing diffuse dark spots. C) Multiple fibers of Bi-hTf and D) faint banding (indicated by arrows) in a Bi-hTf fiber. E) Deglycosylated holo-hTf showing fibers with uniformly spaced dark spots. F) Shorter fibers of deglycosylated holo-hTf.

Serum transferrin is thought to be a natural transporter for manganese (probably as Mn^{III}) in the body and binds Bi^{III} (e.g. from antiulcer drugs) strongly in the iron-binding sites.[6,16–18] The micrographs of manganese- and bismuth-loaded apo-hTf once again revealed the occurrence of electron-dense regions in the fibrils (Figure 4 B–D and Figures S8 and S9 in the Supporting Information), albeit with a periodicity different from that of the iron-loaded hTf. It can be concluded therefore that the nature of the metal bound to transferrin also has a direct influence on nanomineralization, presumably through the kinetics of the processes and the structure and stability of the different minerals formed.

We next investigated whether the glycan chains attached to transferrin play a role in fiber formation. Human transferrin contains two biantennary glycan chains attached to asparagine 413 and asparagine 611 in the C-lobe. TEM micrographs of deglycosylated holo-hTf (1 μM, 5 mM NH_4HCO_3, pH 7.4) also showed the presence of uniformly spaced dark spots with an average spacing comparable to the glycosylated protein (Figure 4 E, F). Therefore, it appears that the sugar chains have little influence on the self-assembly process that leads to fiber formation and nanomineralization, other than subtly influencing the morphology of the fibers. Critical protein–protein interactions therefore probably involve surface regions of transferrin remote from Asn413 and Asn611, perhaps in the N-lobe.

It is interesting to consider possible mechanisms for fiber formation by holo-hTf and of nanomineralization. Deposition on surfaces seems to have little effect on the integrity of the protein. Transferrin does not readily denature, remaining folded down to approximately pH 4.3 whereupon it forms molten-globule states.[19] It seems likely that aggregation is initiated by relatively small changes in protein structure, for example a change in the relative orientation of the two lobes. Such structural flexibility is important to the natural biological activity of transferrin. Upon binding to the transferrin receptor, holo-hTf straightens, and the relative position of the two hTf lobes changes by approximately 9 Å, a process which is thought to facilitate iron release.[20] Such a structural change may be driven in the present case by dehydration on the surface. Release of bound carbonate and loss as volatile CO_2 could readily lead to the formation of cavities in which confined crystallization of iron hydroxide/oxide can occur. Freeze-drying of ovotransferrin is believed to cause a change in the mode of binding of carbonate from bi- to monodentate.[21] Fiber formation may involve interaction between the tips of the two N-lobe domains in much the same way as in the dimers found in the X-ray crystal structure of human apo-Tf.[22] The two lobes of hTf are connected by a short connecting peptide Thr330–Pro341, and an interlobe disulfide bridge Cys331–Cys402 constrains some interlobe movement.

An interesting hypothesis is that hydroxo/oxo iron species released from the protein during the rapid dendritic outgrowth accumulate at the growing tips of the fibers until

supersaturation is reached, and then mineralization occurs. Further cycles could then give rise to waves of growth and deposition and the episodic and sometimes periodic patterns observed.[23] Since the dimensions of transferrin are approximately 8×10 nm, some 50–100 or more protein molecules probably span the width of the observed fibers.

It will be interesting to investigate whether fibril formation and nanomineralization by holo-transferrin can occur in tissues and, in particular, contribute to the processes responsible for the abnormal accumulation of iron in the brain that is thought to play a role in neurodegenerative diseases such as Parkinson's, Huntington's, and Alzheimer's.[3,24] Highly reactive iron sites can induce formation of toxic free radicals (reactive oxygen species, ROS), which attack neurons. Such a molecular understanding of iron deposition could lead to the design of agents that disrupt hTf aggregation and form a basis for the design of new drugs. The ability of proteins to alter their conformation and give rise to fibril (amyloid) formation is a topic of widespread biological and medical interest.[25]

Experimental Section

Materials: Human holo-transferrin (hTf; cat. no. T4132), apo-transferrin (cat. no. T1147), and dialysis tubing were purchased from Sigma–Aldrich. Ferric chloride, bismuth subcarbonate, nitrilotriacetic acid, sodium bicarbonate, and HEPES (4-(2-hydroxyethyl)-1-piperazineethanesulfonic acid) buffers were purchased from Sd-Fine Chemicals India. Fe(NTA) and Bi(NTA) were synthesized as reported.[26–29]

Metal reloading: To reload with iron or bismuth, apo-hTf (1 μM) was incubated at 37 °C with Fe(NTA) or Bi(NTA) (3 mol equiv) in 10 mM HEPES and 5 mM $NaHCO_3$ solution at pH 7.4 for two days. These solutions were then extensively dialyzed (using Sigma–Aldrich (Z368474–10EA) disposable dialyzers, MWCO 8000 Da, size 1 mL, diameter 5 mm, regenerated cellulose membrane) against 5 mM sodium bicarbonate solution and used for transmission electron microscopy.

Apo-hTf was reloaded with manganese using manganese citrate. The manganese citrate solution was prepared by mixing $MnCl_2$ with triammonium citrate (1:1 molar ratio), adjusting the pH value to 9.0 and stirring for 1 h. A tenfold molar excess of freshly prepared manganese citrate was added to a solution of apo-hTf (100 μM) in 50 mM Tris–HCl buffer (Tris = tris(hydroxymethyl)aminomethane) and 5 mM $NaHCO_3$ (pH 8.0) and incubated for 2 h at 37 °C. The volume of the solution was then reduced from 2 mL to 0.5 mL, and unbound manganese was separated on a Pharmacia PD-10 column. Inductively coupled plasma mass spectrometry (ICP-MS) analysis showed that 2.2 mole manganese atoms were bound per mole protein.

In general, all the metal-loaded proteins were purified on an Akta fast protein liquid chromatography (FPLC) system using a Hi-trap capto-Q column eluted with a linear NaCl gradient. The transferrins in Tris–HCl buffer, pH 8.0 were eluted with 120–140 mM NaCl.[22]

Deglycosylation of holo-hTf: Deglycosylation of the holoprotein was carried out using a modified literature procedure,[30] as the literature procedure was for denatured holoprotein. Commercial lyophilized holoprotein (5 mg) was dissolved in 50 mM phosphate buffer (2 mL), 5 μM dithiothreitol, pH 8.5. PNGase-F (4 μL, 500000 U mL^{-1}) was added and incubated for eight days at 37 °C. The deglycosylated and native proteins were separated using immobilized concanavalin-A. The yield of the deglycosylated protein (based on $\varepsilon_{280} = 93000\ M^{-1}cm^{-1}$) was 1.8 mg. Gel electrophoresis showed the absence of protein cleavage during the glycosylation (see Figure S10 in the Supporting Information). ESI mass spectrometry of the deglycosylated protein gave a mass of 75144 Da (calcd for apo-deglycosylated protein 75141 Da; see Figure S11 in the Supporting Information).

Stability on surface: Samples of apo-transferrin, holo-transferrin, Mn-loaded transferrin and deglycosylated holo-transferrin (5 μM) in 5 mM NH_4CO_3 were incubated at 37 °C for 48 h. Drops (5 μL) were then dried on a glass slide at either 20 °C or 37 °C and extracted from the plate using the SDS (sodium dodecyl sulfate) gel loading buffer. After heating on a boiling water bath for 3 min they were brought to ambient temperature and then loaded on a 12% bis-Tris gel (Invitrogen; Figure S13 in the Supporting Information).

Scanning electron microscopy (SEM): Solutions of protein (1 μM) in deionized water or bicarbonate buffer (1 mM, pH 7.21) were incubated at 37 °C for 0–7 days. Aliquots (10 μL) were loaded onto copper stubs. After drying, the sample was gold-coated, and subsequent SEM and EDX measurements were performed on an FEI QUANTA 200 microscope equipped with a tungsten filament gun and an EDAX EDX detector. Micrographs were recorded at working distance (WD) of 10.6 mm.

Atomic force microscopy (AFM): Solutions of protein (1 μM) in deionized water or 1 mM bicarbonate buffer were incubated at 37 °C for 0–7 days. Aliquots (6 μL) were transferred onto freshly cleaved mica surfaces and uniformly spread with the aid of a spin-coater operating at 200–500 rpm (PRS-4000). The sample-coated mica was dried for 30 min at room temperature and subsequently imaged with an atomic force microscope (Molecular Imaging, USA) operating under acoustic AC mode (AAC), with the aid of a cantilever (NSC 12(c) from MikroMasch). The force constant was 0.6 $N\,m^{-1}$, while the resonant frequency was 150 kHz. The images were taken in air at room temperature, with scan speeds of 1.5–2.2 lines per second. Data were acquired using PicoScan 5 software, while the data analysis was carried out with visual SPM.

Transmission electron microscopy (TEM): Proteins were dissolved in deionized water or 1, 5, or 25 mM bicarbonate buffer with subsequent incubation at 37 °C from 0–7 days. Aliquots (5–6 μL) were loaded onto formvar-coated (Fluka, Switzerland) copper grids and carbon-coated copper grids (SPI supplies, West Chester, USA, 200 mesh). The sample solution was dried in air at room temperature. After drying, the sample was negatively stained with 2% uranyl acetate for 2 min; excess uranyl acetate solution was absorbed on blotting paper. The sample was air dried and subsequently examined under a JEOL 2000FX-II electron microscope, operating voltage 100 kV.

Optical microscopy: Holo-transferrin was dissolved in deionized water or 1, 5, or 25 mM bicarbonate buffer with subsequent incubation at 37 °C from 0–7 days. Aliquots (10 μL) of the sample were loaded on glass slides and images captured using a LABOMED optical microscope with 40× magnification.

Received: December 13, 2007
Published online: February 5, 2008

Keywords: bioinorganic chemistry · iron · metalloproteins · mineralization · transferrin

[1] S. Mann, *Biomineralization: Principles and Concepts in Bioinorganic Materials Chemistry* Oxford University Press, Oxford, **2001**.
[2] J. Webb, D. J. Macey, W. Chua-anusorn, T. G. St. Pierre, L. R. Brooker, I. Rahman, B. Noller, *Coord. Chem. Rev.* **1999**, *190–192*, 1199 – 1215.
[3] R. R. Crichton, R. J. Ward, *Metal-based Neurodegeneration: From Molecular Mechanisms to Therapeutic Strategies*, Wiley, Chicester, **2006**.
[4] N. D. Chasteen, P. M. Harrison, *J. Struct. Biol.* **1999**, *126*, 182 – 194.

[5] P. Aisen, C. Enns, M. Wessling-Resnick, *Int. J. Biochem. Cell Biol.* **2001**, *33*, 940 – 959.
[6] P. J. Sadler, H. Li, H. Sun, *Coord. Chem. Rev.* **1999**, *185–186*, 689 – 709.
[7] E. N. Baker, P. F. Lindley, *J. Inorg. Biochem.* **1992**, *47*, 147 – 160.
[8] H. Zhu, D. Alexeev, D. J. Hunter, D. J. Campopiano, P. J. Sadler, *Biochem. J.* **2003**, *376*, 35 – 41.
[9] S. R. Shouldice, R. J. Skene, D. R. Dougan, D. E. McRee, L. W. Tari, A. B. Schryvers, *Biochemistry* **2003**, *42*, 11908 – 11914.
[10] W. Zhong, D. Alexeev, I. Harvey, M. Guo, D. J. Hunter, H. Zhu, D. J. Campopiano, P. J. Sadler, *Angew. Chem.* **2004**, *116*, 6040 – 6044; *Angew. Chem. Int. Ed.* **2004**, *43*, 5914 – 5918.
[11] D. Alexeev, H. Zhu, M. Guo, W. Zhong, D. J. Hunter, W. Yang, D. J. Campopiano, P. J. Sadler, *Nat. Struct Biol.* **2003**, *10*, 297 – 302.
[12] We thank Matthew Turner for this suggestion. For the relationship of twisting to stability of sickle hemoglobin fibers, see: M. S. Turner, R. W. Briehl, F. A. Ferrone, R. Josephs, *Phys. Rev. Lett.* **2003**, *90*, 128013.
[13] A. Manceau, J. M. Combes, *Phys. Chem. Min.* **1988**, *15*, 283 – 295..
[14] D. Mavrocordatos, D. Fortin, *Am. Mineral.* **2002**, *87*, 940 – 946.
[15] K. Mizutani, H. Yamashita, H. Kurokawa, B. Mikami, M. Hirose, *J. Biol. Chem.* **1999**, *274*, 10190 – 10194.
[16] J. A. Roth, *Biol. Res.* **2006**, *39*, 45 – 57.
[17] H. Li, P. J. Sadler, H. Sun, *J. Biol. Chem.* **1996**, *271*, 9483 – 9489.
[18] R. Ge, H. Sun, *Acc. Chem. Res.* **2007**, *40*, 267 – 274.
[19] G. Kubal, P. J. Sadler, A. Tucker, *Eur. J. Biochem.* **1994**, *220*, 781 – 787.
[20] Y. Cheng, O. Zak, P. Aisen, S. C. Harrison, T. Walz, *Cell* **2004**, *116*, 565 – 576.
[21] S. S. Hasnain, R. W. Evans, R. C. Garratt, P. F. Lindley, *Biochem. J.* **1987**, *247*, 369 – 375.
[22] J. Wally, P. J. Halbrooks, C. Vonrhein, M. A. Rould, S. J. Everse, A. B. Mason, S. K. Buchanan, *J. Biol. Chem.* **2006**, *281*, 24934 – 24944.
[23] We thank a referee for this suggestion.
[24] L. Zecca, M. B. H. Youdim, P. Riederer, J. R. Connor, R. R. Crichton, *Nat. Rev. Neurosci.* **2004**, *5*, 863 – 873.
[25] C. M. Dobson, *Nature* **2003**, *426*, 884 – 890.
[26] W. Clegg, A. K. Powell, M. J. Ware, *Acta Crystallogr. Sect. C* **1984**, *40*, 1822 – 1824.
[27] S. Toyokuni, K. Uchida, K. Okamoto, Y. Hattori-Nakakuki, H. Hiai, E. R. Stadtman, *Proc. Natl. Acad. Sci. USA* **1994**, *91*, 2616 – 2620.
[28] P. Aisen, A. Leibman, H. A. Reich, *J. Biol. Chem.* **1966**, *241*, 1666 – 1671.
[29] S. P. Summers, K. A. Abboud, S. R. Farrah, G. J. Palenik, *Inorg. Chem.* **1994**, *33*, 88 – 92.
[30] J. S. Padda, A. B. Schryvers, *Infect. Immun.* **1990**, *58*, 2972 – 2976.

